INTL JOURNAL OF ELECTRONICS AND TELECOMMUNICATIONS, 2018, VOL. 64, NO. 4, PP. 487-494
Manuscript received February 21, 2018; revised October, 2018. DOI: 10.24425/123550

The Positioning Accuracy Based on the UWB Technology for an Object on Circular Trajectory

Damian Grzechca, and Krzysztof Hanzel

***Abstract*—This paper presents the comparison of filtering methods – median filtration, moving average Kalman filtration and filtration based on a distance difference to determine the most accurate arm length for circular motion, as a model of wind turbine propellers movement. The experiments have been performed with the UWB technology system containing four anchors and a tag attached to 90cm arm that was rotated with speed up to 15.5 rad/s (as a linear speed of 50km/h). The trilateration concept based on the signal latency has been described in order to determinate the position of an object on circular trajectory. The main objective is the circle plane rotation (parallel and perpendicular) with respect to the anchors plane reference system. All research tasks have been performed for various cases of motion schemes in order to get the filtration method for object in motion under best accuracy goal. Filtration methods have been applied on one of two stages of the positioning algorithm: (1) on raw data got from the single anchor-tag (before trilateration); (2) on the position obtained from four anchors and tag (after trilateration). It has been proven that the appropriate filtering allows for higher location accuracy. Moreover, location capabilities with the use of UWB technology – shows prospective use of positioning of objects without access to other positioning forms (ex. GPS) in many aspects of life such as currently developing renewable, green energy sources like wind turbines where the circular motion plays an important role, and precise positioning of propellers is a key element in monitoring the work of the whole wind turbine.**

***Keywords*—Ultra-Wideband, UWB, localization, propellers positioning, trilateration, location filtration**

I. Introduction

IN a world that cares for environmentally friendly solutions and renewable energy sources, wind farms play a significant role. Circular motion occurring in wind turbines is natural here, and tracking the propellers can help in monitoring work and performing maintenance-free revisions. However, such a solution requires appropriate technologies and tailor-made algorithms. The location of an object in motion especially when object is moving around a circle is not a trivial task and therefore it should be investigated with special attention.

Determination of objects positions can be done using many different techniques, they can be based on the signal strength indicator, wave propagation latency, phase shift, etc. [5], [6], [7]. There are also many factors that need to be met when comparing locating systems. The most important metrics are: accuracy, availability, coverage area, scalability, cost and security, but it can also specify robustness, integrity, update rate, infrastructure, intrusiveness, approval, market maturity, or number of users [8] [3].

To position objects on medium distances, we can use one or more of these technologies: Wireless Local Area Network (WLAN) [9], Cellular Networks[10], Bluetooth [11], [12], Radio Frequency Identification (RFID) [13], Infrared (IR), Ultrasonic, ZigBee, Image Based Technologies, Pseudolites [14] and the Ultra-Wideband (UWB) [15]. All those techniques can be combined with micro electro-mechanical system (MEMS) sensors [16], [17]. This paper focused on Ultra-Wideband, as a most promising technology, which allows objects to be tracked with centimeters accuracy [18].

Many papers focus on selected metrics [19] and the most common approach is people location [20]. In the case of people, there is weak pressure on high precision [21,22] and computational costs [23] and time to first fix are not critical [24], so it is difficult to look for a solution capable of positioning fast-moving propellers.

However, the proposed solution is not only suitable for positioning propellers, but also can be implemented in a relatively low cost devices (with limited computation resources) like unmanned aerial vehicles [25], indoor transportation systems as biomedical, and hospitals cargo, patients monitoring [26] or storage facilities, smart vacuum cleaners, and the increasingly popular small personal electric vehicles as boards, hoverboards or scooters in a smart cities [27,28]. It can also replace current solutions like determining coarse positioning of mobile devices that play a central role in a Smart City, through advertising purposes [1] and using GPS system to navigate systems and to ADAS (Advanced Driver Assistance Systems [2]) as a full stack real time car positioning system.

The authors present a research on easy implementable and low computations cost filtering methods for an object in circular motion with speed up to 50km/h. The current literature does not touch the subject of determining the convergence of surfaces, in contrast to method presented in this article, that allows to determine the length of the arm and the way it goes through with a very good result.

II. Locating System Description

This section presents fundamental and essential information about the system applied. The system has been developed by the team based on the resources available on the decaWave web page [29]. The system is composed of 4 anchors and a Tag (see fig. 1). The system has been built with STM32 Discovery development boards and modules DWM1000. It operates across a wide variety of markets, including ePOS and retail, automotive, agriculture, building control and

This work was supported by the Ministry of Science and Higher Education funding for young researchers statutory activities in 2018 (BKMN 2018).

Authors are with Faculty of Automatic Control, Electronics and Computer Science, Silesian University of Technology, Gliwice, Poland (e-mail: Damian.Grzechca@polsl.pl, Krzysztof.Hanzel@polsl.pl).

automation, factory automation, healthcare, safety and security, warehousing and logistics and a range of others.

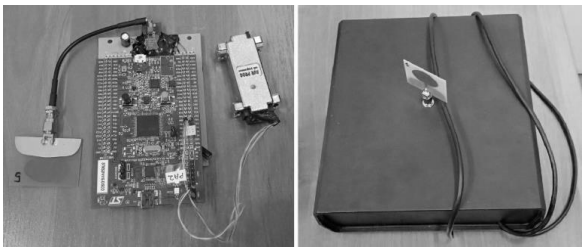

Fig. 1. UWB environment – tag for data acquisition (left), an anchor serves as a station (right)

A. *Description of the equipment and the experiment*

The test stand environment consists of a UWB tag that was receiving and processing signals, as well as four UWB anchors serves as a station with a fixed declared position (fig. 1). All devices are integrated with DWM module consisted of decaWave devices DWM1000 that is an IEEE802.15.4-2011 UWB compliant wireless transceiver. As decaWave declare DWM1000 module are optimized for unrivalled (up to 10 cm) indoor precision location and high communications data rate (up to 6.8 Mb/s) for Real Time Location Systems (RTLS) and Wireless Sensor Networks (WSN).Test stand has been composed of four anchors that were placed on a square with a side length of 500 cm, as shown in fig. 2.

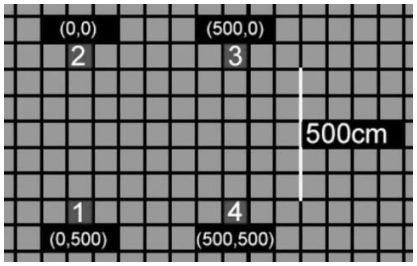

Fig. 2. Research area - location of individual UWB anchors, including coordinates of points (X,Y)

The tag has been attached to the arm of length 100 cm. The complete arm has been attached to an engine which was responsible for fast movement. The idea of the rotation scheme has been presented in the fig. 3. The tag antenna was connected 10 cm from the edge of the arm.

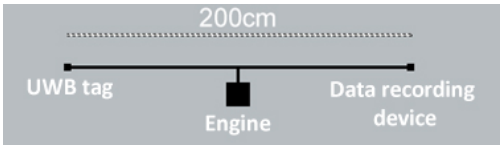

Fig. 3. Diagram of a test bench for measuring the accuracy of circular motion - propeller

The whole process has been performed in 3D environment however chosen metrics have been defined in 2D (as a projection from 3D into 2D), e.g. the expected surface of the circle in 2D is 2.545 m^2 (the tag antenna has been placed 90 cm from the center). It must be emphasized that the observer has been placed parallel to the rotation surface and the axis passing through circle center and the observer is perpendicular to the rotation surface.

The test stand allows for reaching the speed up to 50 km/h (the average speed during the experiment is 50 km/h). It has been assumed two test scenarios: first, the rotation was parallel to the line through anchors 2 and 3 (perpendicular to the line through anchors 1 and 2, towards 2 and 3); second, the rotation was parallel to the line through anchors 1 and 2 (perpendicular to the line through anchors 2 and 3, towards 1 and 2). The fixed point of an engine in 3D environment was at point X,Y,Z (250, 250, 200). The exemplary case has been shown in the fig. 4.

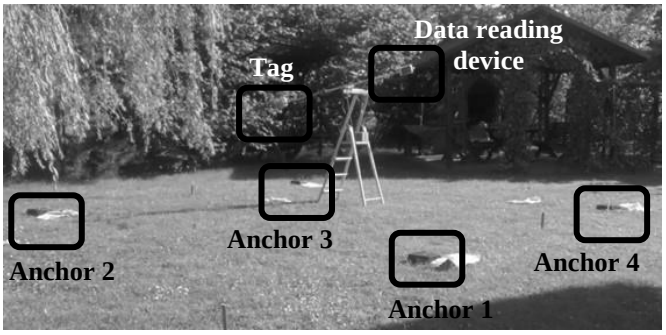

Fig. 4. Real environment with 4 anchors and Tag

The signal processing research process, from the preparation of the test stand up to the processing of results is presented in fig. 5. Filters used with their parameter configurations are described in subsection II.D.

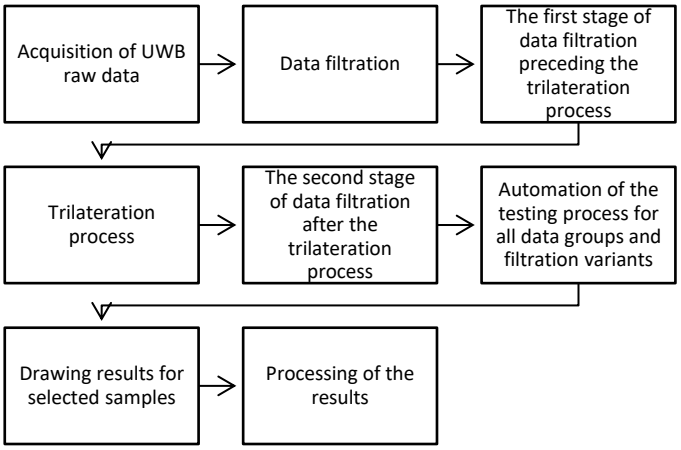

Fig. 5. A diagram showing the course of the study

B. *Description of the acquired data*

During the experiment, two test series were carried out:

1. Label $\mathbf{E}_1$ - a test at XYZ {250.250.200} with a propeller running parallel to the line through anchors 2 and 3 (perpendicular to the line through anchors 1 and 2, towards 2 and 3)
2. Label $\mathbf{E}_2$ – a test at XYZ {250.250.200} with a propeller moving parallel to the line through anchors 1 and 2 (perpendicular to the line through anchors 2 and 3, towards 1 and 2)

Each series consisted of frames - F_i (for i=1…N) containing information about time, marker distance, signal quality and RSSI. The example frame is presented as follows:

```
Fi={47172911;188;326;325;187;
-73.31;-73.55;-76.53;-
0.08;6.95;14.55;6.75;13.04;}
```

The frame is interpreted in the following manner:

F_i = {TS; S_1; S_2; S_3; S_4;
SS_1; SS_2; SS_3; SS_4;
QI_1; QI_2; QI_3; QI_4;}

E = {$F_1, F_2, F_3, \ldots, F_N$}

Where

- N – Total number of data received from the UWB locating system
- TS - time stamp (it is counted from the system start)
- S_1 – S_4 – measured distances between Tag and the following Anchors (in cm)
- SS_1 – SS_4 – signal strength indicator for the following anchors with respect to the Tag (in dBm)
- QI_1 – QI_4 - quality indicator for all anchors; no unit, values between 0 and 1 – the best quality

The tag distance to a reference point (an anchor) for a test scenario (e.g. label E_1) can be represented by the graph, which is shown in fig. 6.

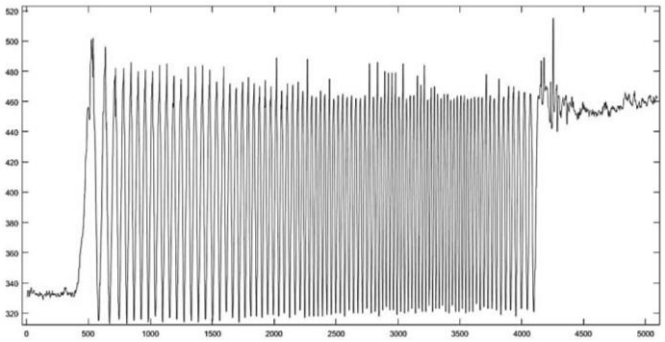

Fig. 6. The rotation of the tag with respect to anchor no 1 for test scenario E1

Full circles have been selected from the whole dataset (for both test scenario) based on the local maxima. A set of single circles has been obtained (pay attention it is raw data obtained from frame **E**):

$$\boldsymbol{C_E} = \{C_1^1, C_1^2, C_1^3, C_1^4, C_2^1, C_2^2, C_2^3, C_2^4, \ldots, C_L^1, C_L^2, C_L^3, C_L^4\}$$

Where: $\boldsymbol{E}$ – is a test scenario label and C_i^j - Upper index j represents anchor number, here 1, …, 4; lower index i represents data set for following circles, here from 1 to L.

C. The trilateration method

The trilateration algorithm has been applied in order to convert the UWB data to a particular position. At the hardware level a TDOA (Time Difference Of Arrival) was implemented. Communication schema is presented in the [14]. Then, the obtained time, also at the hardware level converted to the distance between particular anchors, and tag, that returns distances in centimetres between the tag and following anchors.

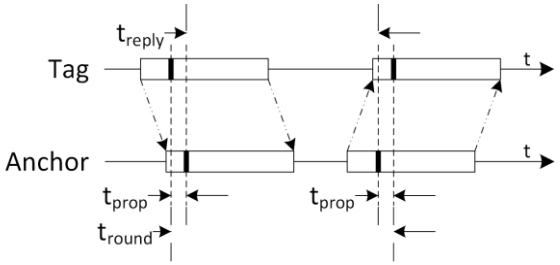

Fig. 7. Communication between UWB Anchor and Tag

The time of flight t_{prop} can be simply calculated with the use of the (1). When the time of flight is known the distance d between anchor and tags can be calculated with the use of the (2).

$$t_{prop} = \frac{t_{round} - t_{reply}}{2} \tag{1}$$

$$d = v \cdot t_{prop} \tag{2}$$

Where v – is the speed of light (299792458 [m/s])

The system (anchor no 1) returns distances in centimeters between the tag and following anchors (datagram F_i). The time stamp should be solid for a single data acquisition – fortunately such requirement is ensured by hardware that performs data acquisition and returns them in packages at specific time intervals.

The principle of operation flows from the fundamental geometry and the main idea is depicted in the fig. 8 [30]. The input data are three (from four available – selection based on RSSI factor) reference points A_1 (x_1, y_1, z_1), A_2 (x_2, y_2, z_2), A_3 (x_3, y_3, z_3) and three distances S_1, S_2, S_3 to point T. To find the coordinates of the point T (x y, z) is equivalent with the determination of the coordinates of the system of quadratic equations shown in (3).

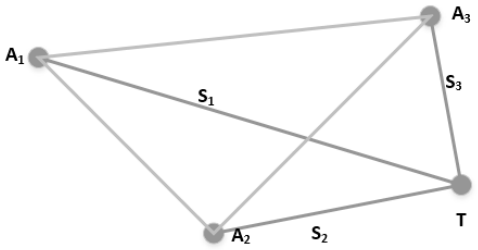

Fig. 8. Trilateration – an example of the operation given for the point - the tag T, and for the three distances S_1, S_2 and S_3 from the three reference points P_1, P_2 and P_3

$$\begin{cases} (x-x_1)^2 + (y-y_1)^2 + (z-z_1)^2 = S_1^2 \\ (x-x_2)^2 + (y-y_2)^2 + (z-z_2)^2 = S_2^2 \\ (x-x_3)^2 + (y-y_3)^2 + (z-z_3)^2 = S_3^2 \end{cases} \tag{3}$$

Equation (3) can be arranged as (4).

$$\begin{cases} (x^2+y^2+z^2) - 2x_1x - 2y_1y - 2z_1z = s_1^2 - x_1^2 - y_1^2 - z_1^2 \\ (x^2+y^2+z^2) - 2x_2x - 2y_2y - 2z_2z = s_2^2 - x_2^2 - y_2^2 - z_2^2 \\ (x^2+y^2+z^2) - 2x_3x - 2y_3y - 2z_3z = s_3^2 - x_3^2 - y_3^2 - z_3^2 \end{cases} \tag{4}$$

Or in matrix representation (5)

$$\begin{bmatrix}1-2x_1-2y_1-2z_1\\1-2x_2-2y_2-2z_2\\1-2x_3-2y_3-2z_3\end{bmatrix}\begin{bmatrix}x^2+y^2+z^2\\x\\y\\z\end{bmatrix}=\begin{bmatrix}s_1^2-x_1^2-y_1^2-z_1^2\\s_2^2-x_2^2-y_2^2-z_2^2\\s_3^2-x_3^2-y_3^2-z_3^2\end{bmatrix} \quad (5)$$

Thus equation (5) is represented in the form (6).

$$\boldsymbol{B_0}\cdot\boldsymbol{x}=\boldsymbol{b_0} \quad (6)$$

With the constraint

$$\boldsymbol{x}\in E$$
$$E=\left\{(x_0,x_1,x_2,x_3)^T\in\frac{\mathbb{R}^4}{x_0}=x_1^2+x_2^2+x_3^2\right\} \quad (7)$$

In our case P_1, P_2 and P_3 do not lie on a straight line so the Rang(B_0) = 3 and dim(Kern(B_0)) = 1. The general solution of (6) is then equation (8).

$$\boldsymbol{x}=\boldsymbol{x}_p+t\cdot\boldsymbol{x}_h \quad (8)$$

Where t is the real parameter, x_p is a particular solution of equation (8) and x_h is a solution of homogeneous system of equations (9), i.e. that is a Basis of Kernel (B_0).

$$\boldsymbol{B_0}\cdot\boldsymbol{x}=0 \quad (9)$$

The x_p and x_h vectors can be determined using the Gaussian elimination method. The particular solution x_p can also be excluded by the pseudo inverse of the matrix B_0.

To determine the parameter t let do (10).

$$\begin{gathered}x_p=(x_{p0},x_{p1},x_{p2},x_{p3})^T\\x_h=(x_{h0},x_{h1},x_{h2},x_{h3})^T\\x=(x_0,x_1,x_2,x_3)^T\end{gathered} \quad (10)$$

After inserted equations (10) through (8) we obtain (11).

$$\begin{cases}x_0=x_{p0}+t\cdot x_{h0}\\x_1=x_{p1}+t\cdot x_{h1}\\x_2=x_{p2}+t\cdot x_{h2}\\x_3=x_{p3}+t\cdot x_{h3}\end{cases} \quad (11)$$

Where we still using the constraint $x\in E$ it follows (12).

$$\begin{gathered}x_{p0}+t\cdot x_{h0}=(x_{p1}+t\cdot x_{h1})^2+\\+(x_{p2}+t\cdot x_{h2})^2+(x_{p3}+t\cdot x_{h3})^2\end{gathered} \quad (12)$$

And thus (13).

$$\begin{gathered}t^2(x_{h1}^2+x_{h2}^2+x_{h3}^2)+\\+t(2\cdot x_{p1}x_{h1}+2\cdot x_{p2}x_{h2}+2\cdot x_{p3}h_{h3}-x_{h0})+\\+x_{p1}^2+x_{p2}^2+x_{p3}^2-x_{p0}=0\end{gathered} \quad (13)$$

This is a quadratic equation in the form $at^2+bt+c = 0$ with the solution as (14).

$$t_{\frac{1}{2}}=\frac{-b\mp\sqrt{b^2-4ac}}{2a} \quad (14)$$

The solutions of the equation system (6) are (15).

$$\begin{gathered}\boldsymbol{x_1}=\boldsymbol{x_p}+t_1\cdot\boldsymbol{x_h}\\\boldsymbol{x_2}=\boldsymbol{x_p}+t_2\cdot\boldsymbol{x_h}\end{gathered} \quad (15)$$

So in the case of 3D positioning using 3 anchors, the position of T_N (XYZ) can be represented as x_1(XYZ) or x_2(XYZ) depending on the expected range of positions in the X Y Z axes.

The choice of the right position was arbitrarily made as a return item in parameter x_1 due to the significant difference between x_1 and x_2 positions, as well as the high distance from the border of those areas that could overlap the spheres received from the UWB system.

D. Filtration methods

As mentioned before, the raw data from the system needs filtration due to noise and environment conditions. For this reason, the following filtrations have been applied on the first or second stage (for both stages if indicated). First stage raw data means distances between an anchor and the tag (frame F), second stage raw data means 3D position after trilateration (tag position T). The following filters have been investigated:

- The median filter. In the research the filter has been applied with the following window size: 1 (as no filtration), 3, 5, 9 and 11, before, and after trilateration. Median with window size k of N_i samples, where $i=1,\dots,k$ and $N_i\le N_i+1$ is presented in equation (16)

$$med(N_i)=\begin{cases}N_{j+1} & for\ k=2j+1\\\frac{1}{2}(N_j+N_{j+1}) & for\ k=2j\end{cases} \quad (16)$$

In this case, the value was always an odd number, so the $k=2_j+1$ was used.

- Kalman filtering (KF), (also known as linear quadratic estimation - LQE), is an recursion algorithm that uses a series of measurements observed over time, containing statistical noise and other inaccuracies, and produces estimates of unknown variables that tend to be more accurate than those based on a single measurement alone [31,32].

The Kalman filter model assumes the true state at time (k) is evolved from the state at $(k-1)$ (17)

$$\begin{gathered}x_k=Ax_{k-1}+w_{k-1}\\z_k=Cx_{k-1}+v_{k-1}\end{gathered} \quad (17)$$

The classical form of a linear-discrete KF is given by prediction shown as (18).

$$\begin{gathered}\hat{\boldsymbol{x}}(k|k-1)=A_k\hat{\boldsymbol{x}}(k-1|k-1)\\P(k|k-1)=A_kP(k-1|k-1)A_k^T+Q_{k-1}\\v_k=z_n-C\hat{\boldsymbol{x}}(k|k-1)\\S_k=C_kP(k|k-1)C_k^T+R\end{gathered} \quad (18)$$

And the filtering process in equations (19).

$$\begin{aligned} K_k &= P(k|k-1)C_k^T(S)^{-1} \\ \hat{\boldsymbol{x}}(k|k) &= \hat{\boldsymbol{x}}(k|k-1) + K_k v_k \\ P(k|k) &= (I_k - K_k C_k)P(k|k-1) \end{aligned} \tag{19}$$

• Moving average types: simple and triangular with window sizes: 1 (as no filtration), 3, 5, 9 and 11 before, and after trilateration.

First, there is calculated the simple moving average (SMA) (20).

$$SMA(T_i) = \frac{1}{k}\sum_{j=-\lfloor\frac{k}{2}\rfloor}^{\lfloor\frac{k}{2}\rfloor} T_j \tag{20}$$

Then, take the average of all the SMA values to get TMA (triangular moving average) values (21).

$$TMA(SMA_i) = \frac{1}{k}\sum_{j=-\lfloor\frac{k}{2}\rfloor}^{\lfloor\frac{k}{2}\rfloor} SMA_j \tag{21}$$

• Pre-processing for discarding points if the current position is further with respect the previous one under maximum speed condition. The subsequent data analysis have been applied for the individual measurement series – for filtration before trilateration for point T and after trilateration for X_T, Y_T Z_T as a current point (as obtained in II C), and J as a filter size the condition (22) is checked.

$$|X_T - X_{T+1}| < J \wedge |Y_T - Y_{T+1}| < J \wedge |Z_T - Z_{T+1}| < J \tag{22}$$

If the above statement is true then the point is further processed. Otherwise (23)

$$X_{T+1} = X_T \wedge Y_{T+1} = Y_T \wedge Z_{T+1} = Z_T \wedge i = i+1 \tag{23}$$

A. Validation methods

The whole process for object localization should be verified with a unified metric. The authors propose validation for the circle projection in two dimensions, z axis is discarded. In order to make projection on the plane, a circle was observed from a point perpendicular to the center of the circle (X Y Z as 250 cm 500 cm 200 cm) with an azimuth equal to 90 and an elevation equal to 0. The following methods of verification are proposed:

• Area of the circle described at the points - used to compare the maximum measurement error outside the test area, relative to the expected area of the circle. Firstly for each points $i, j \in N$, where N was number of all the distance between the furthest points, and the p_{near} and p_{far} as the furthest points was determined (24).

$$\begin{aligned} P_{near} = N_{x_i,y_i} \wedge P_{far} = N_{x_j,y_j} \leftrightarrow \\ \max(dist) = \sqrt{(x_i - x_j)^2 + (y_i - y_j)^2} \end{aligned} \tag{24}$$

From the distance the r was obtained (25) and the center of the circle – $O_{(x,y)}$ (26).

$$r = \frac{dist}{2} \tag{25}$$

$$O_{(x,y)} = \left(\frac{p_{near} + p_{far}}{2}, \frac{p_{near} + p_{far}}{2}\right) \tag{26}$$

• Area of circle fitted to the points by the least squares method - used to compare the measurement error of the circle seen straight ahead of the expected area of the circle.

For two dimensional matrix $\boldsymbol{M}$ of X_N,Y_N the mldivide operation that solve systems of linear equations with (x^2, y^2) was performed, next the center of the circle values S_x and S_y values was obtained as a $O_x = 0.5 * \boldsymbol{M}(1)$, $O_y = 0.5 * \boldsymbol{M}(2)$, and the radius (27)

$$r = \sqrt{\frac{O_x^2 + O_y^2}{4}} - a_3 \tag{27}$$

• Area of ellipse fitted to the points by the least squares method - used to compare the measurement error of the circle seen from the perspective of the observer, relative to the expected area of the circle.

• Area of polygon escribed at the points - Used to compare the measurement error of the received polygon in relation to the expected area of the circle. To get the polygon, the convex hull was used. The convex hull of a set of points O in n dimensions is the intersection of all convex sets containing O. For N points $p_1, \dots, p_N$, the convex hull C is then given by the expression (28)

$$C = \left\{ \sum_{j=1}^{N} \lambda_j p_j : \lambda_j \geq 0 \; for \; all \; j \; and \; \sum_{j=1}^{N} \lambda_j = 1 \right\} \tag{28}$$

• The circle area is calculated by using equation (29).

$$AR_{circle} = 2\int_{-r}^{r} \sqrt{r^2 - x^2}\,dx \tag{29}$$

• The ellipse area is calculated for a as a half of longer radius and b as a half of shorter radius by using equation (30):

$$AR_{ellipse} = 4\int_{0}^{a} b\sqrt{1 - \frac{x^2}{a^2}}\,dx \tag{30}$$

• The polygon area is calculated by using equation (31).

$$AR_{polgon} = \frac{1}{2}\left|\sum_{i=0}^{n-1}(x_i y_{i+1} - x_{i=1} y_i)\right| \tag{31}$$

III. Results and Discussion

The E_1 data set was divided into C_i circles, where $i = 1, \dots, 87$ and the E_2 data series was divided into Ci circles, where $i = 1, \dots, 115$ which have been subjected to filtration. Selected results for median filtration combined with the results obtained for ellipse area are as follows:

TABLE I
VARIANCE OF ELLIPSE SURFACE AREA FOR 87 CIRCLES FROM DATA SERIES E_1 FILTERED BY MEDIAN FILTER WITH STEP FROM 1 TO 11 FOR C AND T DATA

		Size of filter window after trilateration (T)					
		1	3	5	7	9	11
Size of filter window before trilateration (C)	1	0.011	0.018	0.018	0.026	0.044	0.067
	3	0.011	0.018	0.017	0.026	0.044	0.067
	5	0.011	0.017	0.015	0.024	0.042	0.065
	7	**0.010**	0.016	0.015	0.018	0.037	0.061
	9	0.012	0.019	0.019	0.024	0.036	0.065
	11	0.025	0.034	0.035	0.037	0.049	0.070

The highest uniformity of readings for the median filter during observation of the ellipse is obtained for filtration with window size 7 before trilateration and without filtration on vectors T. Average surface area based on experiment E_1, i.e. 87 circles in this point was 1.872 m^2 what is equivalent of 77 cm long arm (inaccuracy equals 13 cm). However it might be noticed, that similar results - 0.011 gives no filtration, and filtration with window 3 and 5 before trilateration without filtration after trilateration. Each of them give similar accuracy. Also noticeable is the decreasing surface with increasing filter window, thus narrowing the circle to the center.

For the second experiment E_2, the number of circles are 115. The best result occurs for filtration with window size 5 before trilateration, i.e. 0.025 with ellipse area 2.439 m^2, what gives 88cm – difference with expected value is 2 cm. As we can see in the fig. *9* visual difference with unfiltered circle (A) and filtered with windows size 5 before trilateration (B) is very small. Difference is in the (C) example was obtained with filter window 7 before, and after trilateration. The arm length calculated from the obtained area in this case is for (A) 86 cm for polygon, 100 cm for circle escribed on points, 85 cm for circle fitted to the points and 85cm for ellipse fitted to the points. Next for the (B) result is analogic: polygon – 86, circle escribed – 100 cm, circle fitted – 85 cm, ellipse fitted – 85 cm. And for the (C): polygon – 78 cm, circle escribed – 95 cm, circle fitted – 81 cm, ellipse fitted – 79 cm.

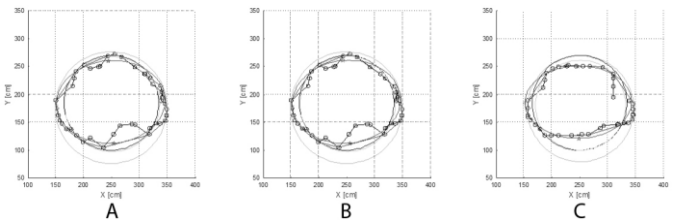

Fig. 9. Filtration results for E2: A – raw data, B – median filter: size 7 for C9 data and size 1 on T9; C – median filter: size 7 for C9 data and size 7 on data T9

Next was performed test based of moving average. Again, the results obtained for the ellipse are presented.

TABLE II
VARIANCE OF ELLIPSE SURFACE AREA FOR 87 CIRCLES FROM DATA SERIES E1 FILTERED BY MOVING AVERAGE WITH STEP FROM 1 TO 11 FOR C AND T DATA.

		Size of filter window after trilateration (T)					
		1	3	5	7	9	11
Size of filter window before trilateration (C)	1	0.011	0.011	0.012	0.015	0.016	0.014
	3	0.013	0.011	0.012	0.015	0.018	0.027
	5	0.011	**0.010**	0.016	0.037	0.240	0.127
	7	**0.009**	0.029	0.079	0.120	0.387	0.157
	9	0.011	0.073	0.142	0.066	0.063	0.151
	11	0.013	0.126	0.096	0.060	0.077	0.098

In case presented in table II, variance of ellipse surface area is smallest also for filtration on C vectors with window size 7 without filtration on T vectors, which corresponds to an average surface area of 1.854 m^2. That is also equivalent of 77 cm long arm, what like in the previous example give 13 cm inaccuracy. Second smallest result is for filtration with window 5 for C, and 3 for T, what gives 1.814 m^2 – average area in this case is equivalent of 76 cm long arm.

For the E_2 data series minimal variance occurred for filtration with window size 5 on C vector – 0.013 with average surface area 2.272 m^2 what is equivalent of 85 cm long arm 5 cm difference from the expected value. Also the circle after filtration with window size 3 on vectors C give in this example similar result – 2.272 m^2.

Kalman filtration was investigated at the third stage. Results are shown in Table III.

TABLE III
THE VALUES OF STATISTICS FOR MEASUREMENT WITH THE KALMAN FILTRATION FOR E_2 DATA SERIES ON T VECTORS

	Polygon *escribed on points*	*Circle escribed on points*	*Circle fitted to the points*	*Ellipse fitted to the points*
Average [area m^2] ***Arm length [cm]***	2.462 89	3.749 109	**2.575** **91**	**2.699** **93**
Variance	0.007	0.042	**0.009**	**0.019**
Median [area m^2] ***Arm length [cm]***	2.459 88	3.775 110	2.576 91	2.703 93
Standard Deviation	0.085	0.205	0.093	0.137
Max [area m^2] ***Arm length [cm]***	2.668 92	4.422 119	2.794 94	2.985 97
Min [area m^2] ***Arm length [cm]***	2.265 85	3.138 100	2.300 86	2.179 83

In this case from the Kalman filtration statistic can be read, that in case of ellipse, but also circle fitted to the points obtained results are most close to the expected ones – respectively 2.699 m^2 for ellipse and 2.575 m^2 for fitted circle what gives 0.93 cm and 0.91 cm long arm. This means that the manufacturer's declared accuracy of up to 10 cm of moving objects up to 18 km/h has been improved up to 3 cm in speed at 50 km/h at a distance of 250 cm from the reference antenna placed at the same height, when we use ellipse fitted to the points, and gives 1cm when we use circle fitted to the points. Also, the worst case from whole test for circle fitted to the

points gives 94 cm and 86cm long arm (4 cm difference from declared), and worst case for the ellipse gives 97 cm and 83 cm long arm what means 7 cm difference from declared length. Another pross of using Kalman filtration in this case has also very low variance – 0.009 for fitted circle and 0.019 for ellipse.

Results of filtering first data series - E_1 using the Kalman filter are presented in the table IV. It can be seen that areas of polygon escribed on points, as well as circle and ellipse fitted to the points are very similar to each other. All three surface areas correspond to the 79 cm – 82 cm long arm. Also for these three values, the biggest inaccurate occur to polygon escribed on the points and is 16 cm. The circle escribed on points, which is the validator of the maximum error for a single dataset, in its maximum value is 3.660 m^2 what is corresponding to the 108 cm long arm – difference from the expected value is 18 cm.

TABLE IV
THE VALUES OF STATISTICS FOR MEASUREMENT WITH THE KALMAN FILTRATION AFTER TRILATERATION FOR E_2 DATA SERIES

	Polygon escribed on points	**Circle escribed on points**	**Circle fitted to the points**	**Ellipse fitted to the points**
Average [area m^2] *Arm length [cm]*	**1.967** **79**	3.380 104	**2.095** **82**	**2.021** **80**
Variance	**0.008**	0.015	**0.005**	**0.012**
Median [area m^2] *Arm length [cm]*	1.968 79	3.379 104	2.097 82	2.006 80
Standard Deviation	0.088	0.123	0.069	0.111
Max [area m^2] *Arm length [cm]*	2.188 83	3.660 108	2.255 85	2.367 87
Min [area m^2] *Arm length [cm]*	1.740 74	3.133 100	1.922 78	1.808 76

In the fig. *10* below, is presented sample result of filtration using Kalman filter. In the (A) figure – filtration without trilateration - result of arm length calculated basing on surface area is 86 cm for polygon, 100 cm for circle escribed on points, 85 cm for circle fitted to the points and 85 cm for ellipse fitted to the points. For the (B) figure it is 87 cm for the polygon (+1 cm to the expected result relative to data without filtration), 103 cm for the circle escribed on the points (-3 cm), 87 cm for the circle fitted (+2 cm) and 87 for the ellipse (+2 cm).

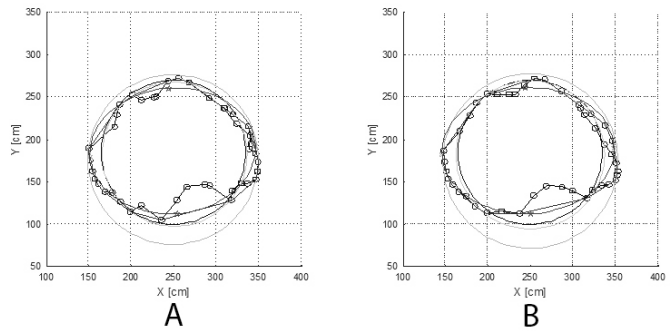

Fig. 10. Graph showing filtration results for median filter of circle no. C_9 in data vector T_2. A shows the result without filtration, and B with Kalman filtration after trilateration.

The last type of tested filtration was filtration based on the difference in distance between points. The result of performed filtration is presented in table V.

TABLE V
VARIANCE OF ELLIPSE SURFACE AREA FOR 87 CIRCLES FROM DATA SERIES E_1 FILTERED BY FILTRATION BASED ON THE DIFFERENCE IN DISTANCE BETWEEN POINTS WITH STEP FROM 1000 (AS NO FILTRATION) DOWN TO 20 FOR BOTH DATA VECTORS

		Size of filter window [cm] after trilateration (T)							
		1000	100	50	40	35	30	25	20
Size of filter window [cm] before trilateration (C)	1000	0.011	0.011	0.011	0.014	0.016	0.011	**0.009**	0.327
	100	0.011	0.011	0.011	0.014	0.016	0.011	**0.009**	0.327
	50	0.011	0.011	0.011	0.013	0.016	0.011	**0.009**	0.270
	40	0.011	0.011	0.011	0.014	0.017	0.016	0.013	0.417
	35	0.012	0.012	0.011	0.015	0.018	0.023	0.075	0.476
	30	0.012	0.012	0.014	0.016	0.018	0.025	0.084	0.925
	25	0.016	0.016	0.024	0.056	0.074	0.181	0.213	1.057
	20	0.183	0.230	0.517	0.430	0.534	0.609	1.329	0.786

In this method we calculate the difference between next points, and if the difference was larger than size of filter window, the point was replaced with previous one. For filtration on C vectors filtration was subjected to the distance between tag and the individual reference points. For filtration on T vectors, the linear distance on the X and Y axis was independently tested. What we can see in the table, is that the filtration on T with window size 25 gives smallest variance – 0.009 what corresponds with surface area 1.925 m^2, 1.925 m^2 and 1.921 m^2 for filter window size 1000 cm – as no filtration, 100 cm and 50 cm. These distances are equivalent of an arm of length 78 cm – 12 cm difference from declared 90 cm. For the E_2 data series smallest variance for the fitted circle was obtained for filtration window 40 cm on vector F and 1000 cm and 100 cm for T what gives area 2.319 m^2 and arm length 86 cm – 4 cm difference from the expected value.

IV. CONCLUSION

Localization of objects in circular motion with the use of UWB technology gives high accuracy in relatively short time. The paper shows influence of chosen filters on localization accuracy under predefined metrics: circle and ellipse, and the radius of real arm which have been compared with one obtained after filtration. In details, median filter accuracy is in range 2% - 14% (i.e. 2 cm – 13 cm) depending on the selected type of motion and samples axis. Moving average filter is less accurate than median filter because the absolute radius minimum error is 6% (i.e. 5 cm). Distance-based filtration accuracy deviates form 6% up to 8% (i.e. 5 cm – 7 cm). The best results give filtration based on Kalman filter – its accuracy is improved from declared 11% (10 cm) up to 1% (1 cm), so the length of the arm is almost equal to the real one.

On the basis of the tests, it can be said that the precision in determining the required length of the arm depends on many factors (speed, position of the observer, type of filtration, surface of motion with respect to anchors). The proposed

metrics, i.e. obtained from the surface area, are well suited to reflect the movement of the UWB tag during the measurement series.

The research schemes investigated in this paper allows for object positioning and object localization with good enough accuracy. It can be applied location of wind turbine propellers for monitoring purposes, but also for indoor and outdoor positioning cases. If other systems, like MEMS are available then the accuracy can be increased. For indoor environment, where GPS signal is weak, the system allows for positioning, i.e. indoor navigation. Such system can be introduced in smart cities as cheap alternative system for object positioning within selected areas, e.g. on crossroads where the accident probability is relatively high.

REFERENCES

[1] Aalto L, Göthlin N, Korhonen J, Ojala T. Bluetooth and WAP Push Based Location-aware Mobile Advertising System. Proc. 2Nd Int. Conf. Mob. Syst. Appl. Serv., New York, NY, USA: ACM; 2004, p. 49–58. doi:10.1145/990064.990073.

[2] Ziebinski A, Cupek R, Erdogan H, Waechter S. A Survey of ADAS Technologies for the Future Perspective of Sensor Fusion. Comput. Collect. Intell., Springer, Cham; 2016, p. 135–46. doi:10.1007/978-3-319-45246-3_13.

[3] Mautz R. Indoor positioning technologies. Habilit Thesis 2012. doi:10.3929/ethz-a-007313554.

[4] Baheti R, Gill H. Cyber-physical systems. Impact Control Technol 2011;12:161–6.

[5] Pittet S, Renaudin V, Merminod B, Kasser M. UWB and MEMS Based Indoor Navigation. J Navig 2008;61:369–84. doi:10.1017/S0373463308004797.

[6] Budniak K, Tokarz K, Grzechca D. Practical Verification of Radio Communication Parameters for Object Localization Module. Man–Machine Interact. 4, Springer, Cham; 2016, p. 487–98. doi:10.1007/978-3-319-23437-3_41.

[7] Nurminen H, Dashti M, Piché, Robert. A Survey on Wireless Transmitter Localization Using Signal Strength Measurements. Wirel Commun Mob Comput 2017. doi:10.1155/2017/2569645.

[8] Alarifi A, Al-Salman A, Alsaleh M, Alnafessah A, Al-Hadhrami S, Al-Ammar M, et al. Ultra Wideband Indoor Positioning Technologies: Analysis and Recent Advances. Sensors 2016;16:707. doi:10.3390/s16050707.

[9] Wang X, Xu K, Li Z. SmartFix: Indoor Locating Optimization Algorithm for Energy-Constrained Wearable Devices. Wirel Commun Mob Comput 2017. doi:10.1155/2017/8959356.

[10] Luo J-N, Yang M-H. Unchained Cellular Obfuscation Areas for Location Privacy in Continuous Location-Based Service Queries. Wirel Commun Mob Comput 2017. doi:10.1155/2017/7391982.

[11] Chruszczyk Ł, Zając A, Grzechca D. Comparison of 2.4 and 5 GHz WLAN Network for Purpose of Indoor and Outdoor Location. Int J Electron Telecommun 2016;62. doi:10.1515/eletel-2016-0010.

[12] Grzechca D, Pelczar P, Chruszczyk Ł. Analysis of Object Location Accuracy for iBeacon Technology based on the RSSI Path Loss Model and Fingerprint Map. Int J Electron Telecommun 2016;62:371–8.

[13] Ni LM, Liu Y, Lau YC, Patil AP. LANDMARC: Indoor Location Sensing Using Active RFID. Wirel Netw 2004;10:701–10. doi:10.1023/B:WINE.0000044029.06344.dd.

[14] Mautz R. Overview of current indoor positioning systems. Geod Cartogr 2009;35:18–22. doi:10.3846/1392-1541.2009.35.18-22.

[15] Haraz O. Why do we need Ultra-wideband? (1). VLSI-Egypt 2012. http://www.vlsiegypt.com/home/?p=518 (accessed July 8, 2017).

[16] Grzechca D, Tokarz K, Paszek K, Poloczek D. Using MEMS Sensors to Enhance Positioning When the GPS Signal Disappears. Comput. Collect. Intell., Springer, Cham; 2017, p. 260–71. doi:10.1007/978-3-319-67077-5_25.

[17] Grzechca D, Wrobel T, Bielecki P. Indoor localization of objects based on RSSI and MEMS sensors, 2014, p. 143–6. doi:10.1109/ISCIT.2014.7011888.

[18] Dardari D, Decarli N, Guerra A, Al-Rimawi A, Puchades V, Mar&#xed C, et al. High-Accuracy Tracking Using Ultrawideband Signals for Enhanced Safety of Cyclists. Mob Inf Syst 2017. doi:10.1155/2017/8149348.

[19] Bernardin K, Stiefelhagen R. Evaluating Multiple Object Tracking Performance: The CLEAR MOT Metrics. EURASIP J Image Video Process 2008;2008:246309. doi:10.1155/2008/246309.

[20] Constandache I, Bao X, Azizyan M, Choudhury RR. Did You See Bob?: Human Localization Using Mobile Phones. Proc. Sixt. Annu. Int. Conf. Mob. Comput. Netw., New York, NY, USA: ACM; 2010, p. 149–160. doi:10.1145/1859995.1860013.

[21] Yang P, Wu W, Moniri M, Chibelushi CC. Efficient Object Localization Using Sparsely Distributed Passive RFID Tags. IEEE Trans Ind Electron 2013;60:5914–24. doi:10.1109/TIE.2012.2230596.

[22] Agrawal M, Konolige K. Real-time Localization in Outdoor Environments using Stereo Vision and Inexpensive GPS. 18th Int. Conf. Pattern Recognit. ICPR06, vol. 3, 2006, p. 1063–8. doi:10.1109/ICPR.2006.962.

[23] Pescaru D, Curiac D-I. Anchor Node Localization for Wireless Sensor Networks Using Video and Compass Information Fusion. Sensors 2014;14:4211–24. doi:10.3390/s140304211.

[24] Lehtinen M, Happonen A, Ikonen J. Accuracy and time to first fix using consumer-grade GPS receivers. 2008 16th Int. Conf. Softw. Telecommun. Comput. Netw., 2008, p. 334–40. doi:10.1109/SOFTCOM.2008.4669506.

[25] Murray CC, Chu AG. The flying sidekick traveling salesman problem: Optimization of drone-assisted parcel delivery. Transp Res Part C Emerg Technol 2015;54:86–109. doi:10.1016/j.trc.2015.03.005.

[26] Grzechca D, Komorowski D, Pietraszek S. A Universal Wireless Device for Biomedical Signals Recording. Pervasive Mob. Sens. Comput. Healthc., Springer, Berlin, Heidelberg; 2013, p. 157–74. doi:10.1007/978-3-642-32538-0_7.

[27] Song U-K, Kim B-K. Development of a DGPS-Based Localization and Semi-Autonomous Path Following System for Electric Scooters. J Inst Control Robot Syst 2011; 17:674–84. doi:10.5302/J.ICROS.2011.17.7.674.

[28] Trulls E, Corominas Murtra A, Pérez-Ibarz J, Ferrer G, Vasquez D, Mirats-Tur JM, et al. Autonomous navigation for mobile service robots in urban pedestrian environments. J Field Robot 2011;28:329–54. doi:10.1002/rob.20386.

[29] ScenSor Module DWM1000 - WSN | decaWave n.d. https://www.decawave.com/products/dwm1000-module (accessed October 19, 2017).

[30] Abdelmoumen Norrdine. An Algebraic Solution to the Multilateration Problem 2015. doi:10.13140/RG.2.1.1681.3602.

[31] Premebida C, Nunes U. Segmentation and geometric primitives extraction from 2D laser range data for mobile robot applications. Robotica 2005;2005.

[32] Breckon T. 2D Target tracking using Kalman filter. 2016.